A

Project Report

On

Studies on Adsorption Isotherms and Heats of Adsorption of CH_4 on Microporous and Mesoporous Adsorbents

Submitted by

K.Bantraj

(Roll No: 107CH003)

In partial fulfillment of the requirements for the degree in

Bachelor of Technology in Chemical Engineering

Under the guidance of

Dr. Pradip Chowdhury

Department of Chemical Engineering

National Institute of Technology Rourkela

May, 2011

CERTIFICATE

It is certified that the work contained in the thesis entitled "*Studies on adsorption isotherms and heats of adsorption of CH_4 on microporous and mesoporous adsorbents*" submitted by Mr. Kandi Bantraj, has been carried out under my supervision and this work has not been submitted elsewhere for a degree.

_____

Date: 09.05.2011

Dr. Pradip Chowdhury

Assistant Professor

Dept. of Chemical Engineering

NIT Rourkela

Acknowledgements

I would like to offer my sincere gratitude to my thesis supervisor, Dr. Pradip Chowdhury for his immense interest and enthusiasm on the project. His technical prowess and vast knowledge on diverse fields left quite an impression on me. He was always accessible and worked for hours with me and I always found his helping hand when it required. He has been a constant source of encouragement for me.

Kandi Bantraj

Roll No: 107CH003

B.Tech., Final Year,

Dept. of Chem. Engg.,

NIT Rourkela

ABSTRACT

In our present area of research we have picked CH_4 as the probe. Methane is a non-polar molecule with a kinetic diameter of 3.8 Å. Methane in 'adsorbed' mode is being projected to be an alternative to compressed natural gas (or, CNG) as fuel in vehicular transportation. It is therefore of paramount importance to find an adsorbent suitable enough for its storage. The two very fundamental things before any adsorbent can be claimed to a suitable one are:

(a) High storage capacity

(b) Fast kinetics

Capacity signifies amount of gas being adsorbed (usually expressed in molar units) per unit mass or volume of adsorbent sample. Kinetics on the other hand explains how fast or slow a gas molecule will be released from the adsorbed phase to the bulk gas phase in desorption cycle. Although several research works in the recent past have published experimental data on CH_4 adsorption (both gravimetry and volumetry) on various adsorbents, but a careful observation would indicate ambiguity. Data published for same experimental conditions on similar adsorbent surfaces varied from lab to lab. More importantly, concrete experimental data of CH_4 on MOF surfaces are limited as compared to other conventional adsorbents. In our present endeavour, we clearly defined our objectives in two fronts:

Firstly, a comprehensive literature survey has been carried out on CH_4 adsorption on several industrially important adsorbents. Judicious interpolation and extrapolation have been carried out wherever required to extract data relevant to particular applications. Efforts are made to ensure uniformity in the 'units' chosen for all cases considered. This is followed by a thorough comparative study.Secondly, we focused our attention to 'novel adsorbent' group, metal organic frameworks or MOFs. We selected two specific type of adsorbent surfaces, Cu-

BTC (or, HKUST-1) is a microporous adsorbent (pore size<2 nm) and Cr-BDC (or, MIL-101) is a mesoporous adsorbent, pore size lying between (2-50 nm). These two adsorbents have gained enormous response in research community owing to their high surface area (850-3500 m^2 g^{-1}) and thermal stability (250-400^oC). We studied in detail CH_4 adsorption data on them. Such a study would certainly help to shed some light on 'adsorbate-adsorbent' interaction at the molecular level. Langmuir model is extensively used in 'fitting' the experimental data. Saturation loading and Henry constants are found from the model parameters.

Key Words: Adsorption, Isotherms, Langmuir Model, Adsorbed Natural gas (ANG)

CONTENTS

LIST OF TABLES

LIST OF FIGURES

LIST OF SYMBOLS

N	Excess amount adsorbed, mmol g^{-1}
A	Specific surface area of the adsorbent, m^2 g^{-1}
a	Specific area of adsorbent per mole of adsorbate, m^2 mol^{-1}
b	Second virial coefficient in adsorbed phase, $mmol^{-1}$ g
b_{ij}	Cross virial coefficients (when $i = j$), $mmol^{-1}$ g
b_{mix}	Second virial coefficient for the mixture in the adsorbed phase, $mmol^{-1}$ g
c	Third virial coefficient in adsorbed phase, $mmol^{-2}$ g^2
c_{ijk}	Cross virial coefficients (when $i = j = k$)
h	Molar enthalpy, kJ mol^{-1}
Δh_{ads}	Enthalpy of adsorption, kJ mol^{-1}
$\Delta h_{ads,0}$	Enthalpy of adsorption at zero loading, kJ mol^{-1}
β	Henry constant, $mmolg^{-1}$ bar^{-1}
β_i	Henry constant for species i in the adsorbed phase, mmol g^{-1} bar^{-1}
k	$-\ln \beta$, where β is Henry constant (units as appropriate)
P	Pressure, bar
R	Universal gas constant, 8.314 J mol^{-1} K^{-1}
T	Temperature, K

GREEK LETTERS

π	Spreading pressure, N m^{-1}
α_{ij}	Separation factor between species i and j
α	Polarizability

CHAPTER 1

Introduction

1.1 Definition and Brief Review

The forces acting on the surface of a solid are unsaturated and hence when the solid is exposed to a gas, the gas molecules associate with the surface through van der Waal's and/or chemical bonds with the solid surface. This phenomenon is known as adsorption [1]. Adsorption can be broadly classified into two categories: physical adsorption or physisorption and chemical adsorption or chemisorption. Physical adsorption involve only relatively weak intermolecular forces (i.e. van der Waals forces) and the physisorbed molecule undergoes no significant change in electronic structure whereas chemisorption involves, essentially, the formation of a chemical bond between the sorbate molecule and the surface of the adsorbent i.e. the molecule's electronic structure is significantly perturbed upon adsorption.

Ever since the concept of adsorption became clearer to the researchers and particularly after the development of synthetic adsorbents and subsequent adsorption based cycles (importantly, PSA and TSA), this particular unit operation has got tremendous response in industrially challenging processes. The most important of them is in the field of 'separation technology'. In the following paragraphs a general review on adsorption is discussed.

All adsorption separation processes involve two principal steps. They are: (a) *adsorption*, when one component is being preferentially adsorbed onto the solid from its mixture and (b) *desorption* or *regeneration*, during which the adsorbent bed is cleaned to be used for the next cycle. Adsorptive separation processes can be categorized on certain principles. They are summarized as [1]:

(I) *Based on mechanism of separation*: Adsorptive separation is achieved by one of the following three mechanisms: steric, kinetic and equilibrium. Steric effect is also known as size-selective sieving. Here the microporous adsorbent allows only the smaller molecule (diameter of the molecule is comparable with the dimension of the micropore) to pass through whereas larger size molecules are totally excluded. Adsorbents e.g. zeolites having uniform pore size distribution shows steric effect. A common example is separation of linear from branched and cyclic hydrocarbons on 5A zeolite. Kinetic separation is achieved due to the differences in diffusion rates of different molecules. It is achieved with adsorbents of varying pore size distribution. A classic example is the separation of N_2 from Air using molecular sieve carbon. Equilibrium separation on the other hand depends on the differences between relative affinities of the adsorbent towards various adsorbates. Majority of the adsorption processes operate through equilibrium mechanism.

(II) *Based on feed composition*: The separation processes may also be divided in the line of feed concentration. Based on feed concentration the separation process may be divided into bulk separation and purification. As had been defined by Keller [1], bulk separation is the point when 10 wt% or more of the mixture is adsorbed. Purification processes are generally separation processes when the components adsorbed are generally present in low concentration, have little economic value and are not recovered.

(III) *Based on method of adsorbent regeneration*: Adsorbents can be regenerated by several mechanisms. Widely used ones include temperature swing adsorption (TSA) cycles, pressure swing adsorption (PSA) cycles, purge gas stripping and displacement desorption. TSA cycles are run on heating-cooling mechanism

whereas PSA process involves steps like: pressurization-adsorption-countercurrent blowdown and countercurrent purge. PSA processes are fast whereas each heating-cooling cycle in a TSA process requires a lot of time and used exclusively for processes, in which the amount of adsorptive gases being processed are small. Apart from TSA and PSA, other regeneration processes include purge gas stripping and displacement desorption. In inert purge gas stripping cycle, the adsorbent is regenerated by passing a non-adsorbing and weakly adsorbing gas through the adsorber without changing the temperature or pressure. The void in the bed is filled with the inert gas upon completion of regeneration. However, in a displacement desorption a gas or vapour that adsorbs about as strongly as the adsorbate is used; regeneration is thus facilitated both by adsorbate partial-pressure reduction and by competitive adsorption of the displacement medium [1]. Displacement desorption process requires more complex scheme of operation and is used only in situations where rest of the processes fail. Some important examples of displacement desorption technique are MOLEX and PAREX processes. The MOLEX process uses the Sorbex simulated moving bed technique (developed by UOP) to recover high purity n-paraffins by continuous adsorptive separation. This technique is similar in concept to liquid chromatography, but carried out on a large commercial scale. UOP's PAREX process is used for the recovery of *para*-xylene from mixed xylenes that offers high product purity, high product recovery, high efficiency and extended adsorbent life. "Mixed xylenes" is a mixture of C_8 aromatic isomers that includes ethyl benzene, *para*-xylene, *meta*-xylene, and *ortho*-xylene. They boil so closely together that separation by distillation is not practical. PAREX process provides an efficient means of recovering *para*-xylene using a zeolitic adsorbent [1-2]

The importance of adsorption based processes can be gauged from situations when other conventional separation processes don't perform efficiently. A few typical cases are given below [1]:

(I) Although process simplicity and scalability is the reason behind popularity of distillation over other unit operations, however when the relative volatility between the key components to be separated is less than 1.2 to 1.5 or even lesser, distillation becomes highly energy intensive and fails when relative volatility is unity. In such cases, alternate separation mechanisms like adsorption yield better result. Adsorption based separation techniques can be highly efficient because of high separation factors achievable between the key components by pragmatic selection of a suitable zeolite. Separation of isomers e.g. n-paraffin from iso-paraffin using 5A molecular sieve, separation of iso-paraffins, iso-olefins from di-n-butylamine using 10X molecular sieve are the examples where adsorptive separation are more effective than distillation [1, 2].

(II) When the component of our interest is present in low concentration and bulk of the feed is of low-value, adsorption is preferred to distillation.

(III) When the two groups of components to be separated are having overlapping boiling ranges, adsorption based separation is effective if they contain chemically or geometrically dissimilar molecules.

1.2 Adsorbents of Industrial Importance

The success and failure of any adsorption based system largely depends on the selection of a proper adsorbent for a particular application. Although literature is crowded with examples of various adsorbents but only a few could last over the ages of technological advances. Some

well-known adsorbents are: silica gel, activated alumina, activated carbon, carbon molecular sieves and zeolites. Each of these adsorbents has certain specific features that have been exploited in various applications ranging from adsorptive separation/purification, ion-exchange and catalysis.

The primary classification between the adsorbents shows two distinct types of surfaces: 'hydrophilic' and 'hydrophobic'. Such type of behaviour can be attributed to the surface polarity (as a result of presence of ions in the structure) of the adsorbents. Polar adsorbents *viz.* zeolites, activated alumina, silica gel etc. show a tremendous affinity towards polar molecules whereas non-polar activated carbon shows little or no affinity towards polar adsorbates. Zeolites owe their hydrophilic nature to the polarity of the heterogeneous surface whereas presence of hydroxyl groups on the surface of silica gel or activated alumina is largely responsible for their 'hydrophilicity' by hydrogen bond formation. These features are particularly important for consideration during equilibrium based separation processes. The fundamental physical properties of the targeted adsorbate molecule like polarizability, permanent dipole moment, quadruple moment, magnetic susceptibility in comparison with the other molecules present in the mixture needs to be examined in detail at first before sorbent design or selection.

The most important feature of any adsorbent material is their porosity. Basically, a highly porous material possess high specific surface area and total pore volume. Pore size distribution is also an important consideration during physical characterization of a porous material. Parameters like bulk density, crush strength and erosion resistance are also important considerations while characterizing any solid adsorbent before practical applications.International Union of Pure and Applied Chemistry (IUPAC) categorized porous materials into three different categories by size: microporous (<2 nm), mesoporous (2-50 nm) and macroporous (>50 nm). Within the microporous regime, there exists a fundamental

difference between different adsorbents. For adsorbents like silica gel, activated carbon or activated alumina there is a distribution of micropore size whereas in a zeolitic adsorbent since the micropore size is controlled by the crystal structure there is virtually no distribution of pore size. This unique feature of zeolites leads to significant results in adsorption properties and set them apart from other conventional adsorbents.

1.3 Research Objectives

Before going into the research objectives, let us carry out a back ground check on this particular field of research. Ever since MOFs have shown tremendous potential (courtesy, porosity), researchers across laboratories have been trying to exploit its extremely high surface area. Adsorptive gas storage appeared to be a viable option because of enormity of void space inside the 3-D structure. For obvious reasons, H_2 and CH_4 appeared to be the front runners.

In our present area of research we have picked CH_4 as the probe. Methane is a non-polar molecule with a kinetic diameter of 3.8 Å. Methane in 'adsorbed' mode is being projected to be an alternative to compressed natural gas (or, CNG) as fuel in vehicular transportation. It is therefore of paramount importance to find an adsorbent suitable enough for its storage. The two very fundamental things before any adsorbent can be claimed to a suitable one are:

(a) High storage capacity

(b) Fast kinetics

Capacity signifies amount of gas being adsorbed (usually expressed in molar units) per unit mass or volume of adsorbent sample. Kinetics on the other hand explains how fast or slow a gas molecule will be released from the adsorbed phase to the bulk gas phase in desorption cycle. Although several research works in the recent past have published experimental data

on CH_4 adsorption (both gravimetry and volumetry) on various adsorbents, but a careful observation would indicate ambiguity. Data published for same experimental conditions on similar adsorbent surfaces varied from lab to lab. More importantly, concrete experimental data of CH_4 on MOF surfaces are limited as compared to other conventional adsorbents.

In our present endeavour, we clearly defined our objectives in two fronts:

Firstly, a comprehensive literature survey has been carried out on CH_4 adsorption on several industrially important adsorbents. Judicious interpolation and extrapolation have been carried out wherever required to extract data relevant to particular applications. Efforts are made to ensure uniformity in the 'units' chosen for all cases considered. This is followed by a thorough comparative study.

Secondly, we focused our attention to 'novel adsorbent' group, metal organic frameworks or MOFs. We selected two specific type of adsorbent surfaces, Cu-BTC (or, HKUST-1) is a microporous adsorbent (pore size<2 nm) and Cr-BDC (or, MIL-101) is a mesoporous adsorbent, pore size lying between (2-50 nm). These two adsorbents have gained enormous response in research community owing to their high surface area (850-3500 m^2 g^{-1}) and thermal stability (250-400^oC). We studied in detail CH_4 adsorption data on them. Such a study would certainly help to shed some light on 'adsorbate-adsorbent' interaction at the molecular level.

CHAPTER 2

Literature Review

Storage of gases in porous adsorbents is new traits that are gaining grounds in the field of adsorption for various applications. It is a long time since scientists and researchers have been looking for an alternate source energy that can replace fossil fuels whose reserve is decreasing at an alarming rate. Molecular H_2 is targeted to be a more viable option. Automobile sector is a major consumer of energy and with the advancement of fuel cell technology, direct on-board use of hydrogen in vehicular transportation is a real possibility. The difficult part is the storage of H_2 in a safe and economical way. Conventional storage mechanisms like high pressure (compression) storage, cryogenic storage or even storage in metal hydrides are found lacking in certain aspects, be in terms of cost, safety or kinetics. Storage of H_2 in porous adsorbents is a subject that is gaining importance in the recent past. Ever since the development of highly porous metal organic frameworks (MOFs) a major focus is shifted towards its ability to store hydrogen. An outstanding property of MOFs that has prompted their study as hydrogen storage candidate is their large apparent surface area and pore volume. Although literature is crowded with research articles on H_2 storage on MOFs but the results are far from encouraging (with a few exceptions) and a disparity between results are conspicuous. The H_2 adsorption capacity on MOFs is falling short of U.S. Department of Energy (DOE) targets. The 2010 energy density targets for hydrogen storage system (including container and necessary components) are 7.2 MJ kg^{-1} and 5.4 MJ L^{-1}, which translates as 6.0 wt% and 45 kg H_2 per m^3 [27].

Methane is the major component of natural gas with a high heat of combustion. It is abundant compared to conventional fossil fuels and emits least amount of CO_2 per unit of heat

produced. Methane, mostly in vehicular transportation is used as compressed natural gas (CNG) and in few cases as liquefied natural gas (LNG). Liquefied natural gas or LNG offers a comparable energy density to that of petrol or diesel but its storage, requiring expensive cryogenic tanks together with boil-off losses has prevented its widespread commercial applications. CNG mode of storage on the other hand requires pressure as high as 200 bar in pressure vessels. The whole process is costly since it requires expensive multistage compression. The concept of adsorbed natural gas (ANG) where the gas is stored as an adsorbed phase in a porous solid can be a viable alternative to CNG. To promote the vehicular application of methane, the U.S. Department of Energy (DOE) has set target for methane storage at 180 v(STP)/v(standard temperature and pressure equivalent volume of methane per volume of the adsorbed material) under 35 bar, near ambient temperature, with the energy density of ANG being comparable to that of CNG used in current practice [8]. MOFs owing to their extraordinary surface area and pore volume are fast becoming a material to reckon with in this field.

Table 2.1: Literature Review of Adsorption on MOFs (A) CH_4 and CO_2 adsorption (B) Hydrogen adsorption

(A)

Researcher	Material	Gas	Work done (Theoretical/ Experimental)	Ref
Eddaoudi et al.	MOF-5, IRMOF-6	CH_4	Showed good capacity at room temperature.	[5]
Bourrelly et al.	MIL-53, 47	CH_4, CO_2	Explained differences in adsorption mechanism where CO_2 adsorption on MIL-53 shows "breathing-effect".	[6]
Millward et al.	MOF-2, MOF-505, MOF-74, HKUST-1, IRMOF-1,3,6,11, MOF-174	CO_2	Provided ample data to show MOFs to the most effective adsorbent to capture CO_2 than any known conventional adsorbents	[7]
Senkovska et al.	HKUST-1, MIL-101, $Zn_2(bdc)_2dabco$	CH_4	Studied high pressure adsorption and concluded HKUST-1 to be the most promising adsorbent	[8]
Llewellyn et al.	MIL-100, 101	CH_4, CO_2	Reported highest uptake for CO_2 on MIL-101 (better activated sample) so far with significant for CH_4 as well.	[9]

(B)

Researcher	Material	Work done (Theoretical/ Experimental)	Ref
Rosi et al.	MOF-5	Adsorbed H_2 up to 4.5 wt% at 78 K and 1% at room temperature and pressure of 20 bar.	[10]
Rowsell et al.	IRMOF-1,8,11,18 & MOF-177	All the measurements were carried out at 77 K and up to atmospheric pressure and H_2 uptake were found to be 13.2, 15.0, 16.2, 8.9 and 12.5 mg g^{-1} respectively.	[11]
Wong-Foy et al.	IRMOF-1,6,11,20 MOF-177,74 HKUST-1	The measurements were carried out at 77 K and pressure up to 90 bar. The saturation capacity varied widely for each MOF.	[12]
Pan et al.	MMOM	Adsorbed up to 1wt% at room temperature and pressure approximately 48 atm.	[13]
Férey et al.	MIL-53	3.2 wt% (Cr^{3+} based) and 3.8 wt% (Al^{3+} based) at 77 K and pressure under 1.6 MPa.	[14]
Latroche et al.	MIL-100, 101	At room temperature capacity was 0.15 wt% with pressure below 7.33 MPa, but at 77 K it goes up to 3.28 wt% at pressure below 2.65 MPa (for MIL-100) whereas for MIL-101 the capacity was as high as 6.1 wt% at 77 K.	[15]

Researcher	Material	Work done (Theoretical/ Experimental)	Ref
Li et al.	MOF-5, IRMOF-8	Demonstrated the concept of dissociation/spillover in hydrogen storage which enhanced the capacity significantly	[16, 17]
Li et al.	HKUST-1, MIL-101	Showed at 77 K and at low pressure HKUST is more effective whereas at room temperature and high pressure MIL-101 is having more capacity.	[18]
Panella et al.	HKUST-1, MOF-5	Compared the adsorption capacity between these two different MOFs. At 77 K and at high pressures MOF-5 stores more H_2 whereas at low pressures Cu-BTC shows more promises	[19]

CHAPTER 3

Adsorption Isotherms & Models

3.1 Equilibrium Adsorption Isotherms

Adsorption of a pure component of gas on a solid at equilibrium can be represented by the following function:

$$N = f(P,T) \tag{3.1}$$

N is theamount adsorbed in cc STP per gm, P is the pressure and T is temperature.

At constant temperature, the amount of gas adsorbed onto a solid surface is only a function of P and is known as adsorption isotherm [1].

The IUPAC classification [2, 6] of adsorption isotherms is shown in Fig. 3.1. Type I isotherm is characteristic of a microporous adsorbent where molecular diameter of the adsorbate molecule matches exactly with the pore diameter of the adsorbent. There is a definite saturation limit to such type of an adsorbent which corresponds to the complete filling of the micropores. Types II, III and VI corresponds to non-porous or macroporous adsorbents whereas types IV and V characterizes mesoporous adsorbents. Isotherms of types II and IV are associated with stronger gas-solid interactions whereas types III and V associated with weaker gas-solid interactions. An isotherm of type IV suggests the formation of multilayer either on a plane surface or on the walls of pores much larger than the molecular diameter of the adsorbate molecule. Isotherms of types II and III characterizes adsorbents with wide range of pore sizes. For such type of adsorbents as the pressure increases adsorption occurs from monolayer to multilayer followed by capillary condensation.

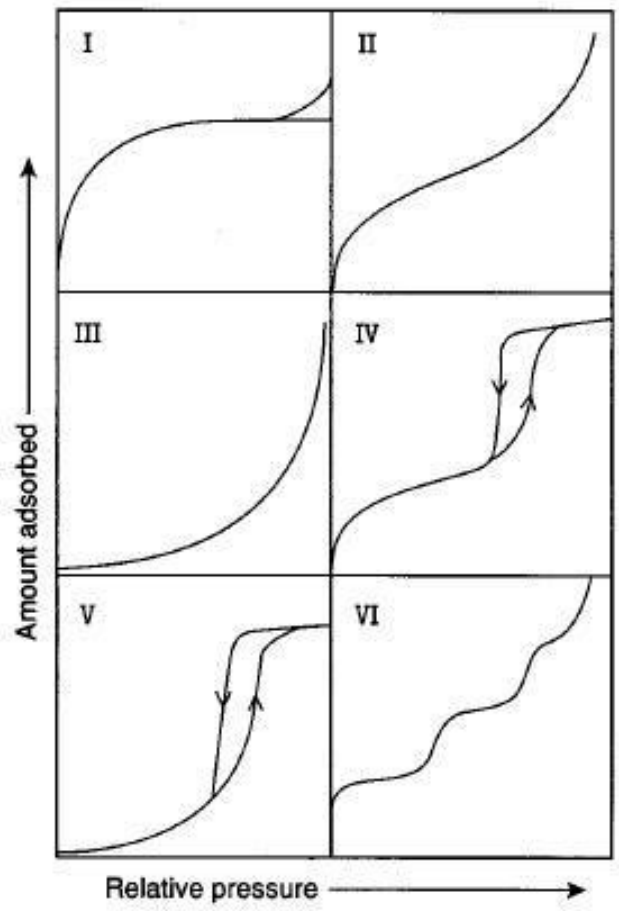

Figure 3.1: IUPAC classifications of adsorption isotherms [3].

3.2 Models for Pure Gas Isotherms

In this section we present a review of various isotherm models used in this work

3.2.1 Langmuir Isotherm

The Langmuir model is based on the following assumptions:

[a] Fixed number of well-defined localized sites

[b] Each site can hold one molecule

[c] All sites are energetically homogeneous

[d] No lateral adsorbate-adsorbate interactions

Based on these assumptions, the Langmuir equation can be represented as

$$N = \frac{N^{\max} HP}{N^{\max} + HP} \tag{3.2}$$

Where, P is the pressure, $N^{\max}$ is the maximum loading corresponding to monolayer coverage and H is Henry constant.

In the above equation, $N^{\max}$ is assumed to be independent of temperature (T), while H is dependent on T and is given by Vant Hoffs' equation of the form

$$H = H_0 e^{-H_1/T} \tag{3.3}$$

3. 2.2 Dual Site Langmuir (DSL) Isotherm

The Dual Site Langmuir (DSL) model is a four-parameter isotherm, distinguishing two categories of different active sorption sites in the adsorbent, each one following a Langmuir adsorption behaviour. The DSL model is represented by [40]

$$N = \frac{N_1^{\max} b_1 P}{1 + b_1 P} + \frac{N_2^{\max} b_2 P}{1 + b_2 P} \tag{3.4}$$

Where, $N_i^{\max}$ and b_i denotes saturation capacity and affinity parameters for sites of type 'i' respectively.

The temperature dependency is included through affinity parameters via

$$b_i = b_i^0 \exp\left[\frac{-\Delta h_{ads}^{(i)}}{R}\left(\frac{1}{T}-\frac{1}{T_0}\right)\right] \tag{3.5}$$

Where, b_i^0 is the affinity at reference at T_0 and $-\Delta h_{ads}^{(i)}$ is the enthalpy of adsorption on site i with respect to temperature T_0.

The Henry's constant in this case is given by

$$H = N_1^{\max} b_1 + N_2^{\max} b_2 \tag{3.6}$$

3.2.3 Virial Isotherm

Based on virial equation of state of the form

$$\frac{\pi a}{RT} = 1 + \frac{b}{a} + \frac{c}{a^2} \tag{3.7}$$

For the two-dimensional surface phase the virial isotherm model can be derived and is represented by

$$\ln(P/N) = k + bN + cN^2 \tag{3.8}$$

e^{-k} Is the Henry constant and is related to the gas-solid interactions only. The other higher coefficients *viz.* b, c etc. are called as second and third virial coefficients respectively.

The temperature dependency of virial coefficients is given by

$$k = k_0 + \frac{k_1}{T} \tag{3.9}$$

$$b = b_0 + \frac{b_1}{T} \tag{3.10}$$

$$c = c_0 + \frac{c_1}{T} \tag{3.11}$$

The physical interpretations of the virial coefficients are strictly valid only for homogeneous adsorbents at low coverage. Since virial equation is open ended, there is no limit on the amount adsorbed as the pressure is increased. But, this can lead to erroneous results if the virial equation is extrapolated beyond the range of data. However, within the temperature and pressure limits of the data, virial equation is flexible and thermodynamically consistent. The virial equation is also reliable to calculate Henry's law constants with good accuracy. In fact in a virial domain plot [$\ln(P/N)$ vs N] or [$\ln(f/N)$ vs N] the intercept is k and is directly related to Henry constant. Henry's constant H is given by

$$H = e^{-k} \tag{3.12}$$

3.2.4 Virial-Langmuir (V-L) Isotherm

The Langmuir equation usually assumes energetic homogeneous surface, rarely possible in realistic situation. On the other hand, virial equation is flexible, thermodynamically correct and describes the heterogeneity of the surface. However, the virial model does not explain the saturation at high pressure, a phenomena observed in many cases.

To overcome this limitation, virial model is modified for an additional term to introduce saturation behaviour at high pressure. The regular isotherm is given by Eq. (3.8) and the modified equation known as Virial-Langmuir isotherm is given by

$$P = \frac{N}{H}\left[\frac{N^{\max}}{N^{\max} - N}\right]\exp[bN + cN^2] \qquad (N < N^{\max}) \tag{3.13}$$

Here, $3/2A^2$ is Henry constant; b , c are virial coefficients; $N^{\max}$ is the saturation capacity [34].

If all the virial coefficients in the Eq. (3.13) are zero, the above expression reduces to the well known Langmuir equation.

The temperature dependency of the parameters H , b and c in this case is given by the following expressions similar to those as described in the preceding paragraph. Saturation capacity $N^{\max}$ is also expressed with similar functionality.

$$N^{\max} = \beta^{\max,0} + \frac{\beta^{\max,1}}{T} \tag{3.14}$$

3.3 Enthalpy of Adsorption

The enthalpy of adsorption, $-\Delta h_{ads}$ is usually obtained from experiments or model parameters using the following equation [34]

$$\Delta h_{ads} = -R\frac{\partial \ln P}{\partial(1/T)} \tag{3.15}$$

Table 3.1 presents equations for enthalpy of adsorption for various models. They are obtained using the Eq. 3.14.

Table 3.1: Enthalpy of adsorption for different isotherm models

Isotherm Models	Enthalpy of Adsorption Equations	Eq. No.
Langmuir	$\Delta h_{ads} / R = H_1$	3.16
Virial	$\Delta h_{ads} / R = k_1 + b_1 N + c_1 N^2$	3.17
Dual SiteLangmuir	$\Delta h_{ads} / R = \frac{\Delta h_{ads}^{(1)} N_1^{\max} b_1 \left(1+b_2 P\right)^2 + \Delta h_{ads}^{(2)} N_2^{\max} b_2 \left(1+b_1 P\right)^2}{N_1^{\max} b_1 \left(1+b_2 P\right)^2 + N_2^{\max} b_2 \left(1+b_1 P\right)^2}$	3.18
Virial-Langmuir	$\Delta h_{ads} / R = k_1 + b_1 N + c_1 N^2 + \frac{N^{\max,1}}{N^{\max}} - \frac{N^{\max,1}}{N^{\max} - N}$	3.19

CHAPTER 4

Experimental Data

All experimental data for our present study were retrieved from literature. '*Windig*' software was used extensively for this purpose. Judicious interpolation and extrapolation was done wherever required. Langmuir isotherm model was used to fit the experimental data. Model fit was carried out using 'MATLAB' (version: 7.3.0.267). Isosteric heat of adsorption equation in the form of 'Clausius-Clapeyron' equation for the Langmuir model was derived and complete derivation is included in the appendix I. Experimental data for CH_4 adsorption on each of the MOFs that we studied too are included in the appendix section. Before proceeding to the next segment let us summarize the physical and electronic properties of CH_4 in tabular form. For better understanding of some of the key features, two more important gases *viz*. O_2 and CO_2 are also included in the table.

Table 4.1: Physical properties of adsorptive gas, CH_4 (* At normal boiling point)

gas	mol. wt. ($g\ mol^{-1}$)	liquid molar volume* ($cm^3\ mol^{-1}$)	Kinetic dia. (Å)	Polarizability ($\times 10^{-25}\ cm^3$)	dipole moment ($\times 10^{18}$ esu. cm)	quadrupole moment ($\times 10^{-40}$ C. m^2)	critical properties	
							pressure (bar)	temperature (K)
O_2	32	28.0	3.5	16.0	0.0	1.3	50.0	154.6
CH_4	**16**	**37.7**	**3.8**	**26.0**	**0.0**	**0.0**	**45.99**	**190.6**
CO_2	44	33.3	3.3	26.3	0.0	14.3	73.83	304.2

CHAPTER 5

Results and Discussions

5.1 Data Analysis

The following table has been compiled after an extensive 'data search' from various relevant literature texts. All data depicted in the table are experimentally found. It is noteworthy to mention that there remains a dearth in experimental data on gas adsorption as compared to simulation data. The gas adsorption data on CH_4 as highlighted in the table are either measured gravimetrically or volumetrically in a high pressure adsorption chamber. Although experimental data were available at various temperatures and pressures, we rather chose a range which is 'realistic', in a sense which sounds industrially feasible.

Column 1 shows the particular adsorbent. Column 2 and 3 are the experimental conditions at which data are collected. Table 4 corresponds to amount adsorbed at that particular pressure at a constant temperature. Column 5 stands for isosteric heat or enthalpy of adsorption. Adsorption is an exothermic process and hence heat is evolved when a particular gas is adsorbed from the bulk gas phase. Had this heat been constant we could have easily interpreted the adsorbent surface to be energetically homogeneous. Since it doesn't remain constant as is visible from the data, we can predict most of the adsorbents studied for CH_4 adsorption are energetically heterogeneous and it changes with loading. Column 6 stands for isosteric heat of adsorption at 'zero' loading. It signifies the very first moment a particular gas molecule interacting with the solid surface. It is always higher than the average heat of adsorption. Henry constant is a parameter that is calculated from the model equations. It signifies the low-pressure zone in the isotherm curve, where the 'loading' is linear with pressure. The last column, 7 are the corresponding references from which all these data are cited.

Table 5.1: Experimental data on CH_4 adsorption on various adsorbents

Adsorbent	Pressure	Temperature	Loading	Isosteric Heat	$q_{st,0}$ (kJ mol^{-1})	Henry constant / H (mmol g^{-1} bar^{-1})	Ref
	P / (bar)	T / K	N / mmol g^{-1}	q_{st} / (kJ mol^{-1})			
13X	25, 50, 89	298	2.84, 3.1, 3.1				[20]
	5, 25, 50	288	1.9, 3, 3.2	17-7	17.53		[21]
	4, 12	298	1.6, 3.6				[27]
4A	92	298	1.56				[20]
5A	84	298	2.91				[20]
5A	1.2, 5.2, 10	303	0.77, 1.46, 1.8	12.97			[33]
AC	5.4, 10.8, 89.7	303	2.4, 3.36, 5				[28]
AC (AS)	5	288	1.6	14.4-7.8	14.35		[21]
AC (BPL)	2.99, 6.52, 37.4	303	1.75, 2.63, 5.1				[22]
AC (Centaur)	2.9, 6.32, 37.3	303	1.75, 2.63, 5.1				[22]
AC (Norit R1)	1.01, 5.04, 57.5	298	1.08, 2.89, 6.4			1.72	[29]
AC (WS42)	2.85, 6.14, 37.3	303	1.82, 2.87, 6.2				[22]
MIL-53 (Al)	5, 10, 25	304	2.2, 3.7, 6.0	17			[6]
BaY	1.07, 5.53, 56	298	0.65, 1.83, 3.9				[36]
CaY	0.96, 6.28, 52.9	298	0.57, 1.95, 4.6				[36]
MIL-53 (Cr)	5, 10, 25	304	2, 3.7, 5.8				[6]
Cu-BTC	6.25, 50, 100	303	5.63, 9.38, 9.5				[8]
	0.94	295	0.92				[37]
	1	295	0.6				[30]
	10, 50	298	5.35, 9.59				[38]

Adsorbent	Pressure	Temperature	Loading	Isosteric Heat	$q_{st,0}$ (kJ mol^{-1})	Henry constant / H (mmol g^{-1} bar^{-1})	Ref
	P / (bar)	T / K	N / mmol g^{-1}	q_{st} / (kJ mol^{-1})			
Cu-BTC	4, 12	298	2.3, 4				[27]
		300			12.5		[31]
Cu-BTC (sample b)	0.9	295	0.8			1.14	[4]
IRMOF-1		300			9.5		[31]
IRMOF-14	10, 50	298	3.57, 12.72				[38]
IRMOF-3		300			12.5		[31]
MCM-41	5, 10, 30	303.15	0.5, 0.95, 2.3				[39]
MgY	0.96, 5.47, 59	298	0.4, 1.69, 4.5				[36]
MIL-100	10, 60	303	3, 9.5	20-9	19	480	[9]
MIL-101	6.25, 50, 100	303	2.5, 7.19, 8.6				[8]
MIL-101 (Sample a)	10, 34, 80	303	3.7, 10, 14.5	18-10			[9]
MIL-101 (Sample b)	10	303	3.7	18-10			[9]
MIL-101 (Sample c)	10	303	3.7	18-10	18	580	[9]
MS (CMS1)	3.09, 4.94, 37.5	303	1.26, 1.52, 2.5				[22]
NaETS-4	1.07	288	0.54	29.3			[23]
NaX	0.93	304.3	0.60	19.2-19.8	19.2		[24]
		304.41			19.2		[25]
NaY	1.24, 6.14, 60.4	298	0.31, 1.59, 4.1				[36]

Adsorbent	Pressure	Temperature	Loading	Isosteric Heat	$q_{st,0}$ (kJ mol^{-1})	Henry constant / H (mmol g^{-1} bar^{-1})	Ref
	P / (bar)	T / K	N / mmol g^{-1}	q_{st} / (kJ mol^{-1})			
Na-ZSM-5	0.83	296.3	0.7	26.5-22.5	26.5		[24]
Silicalite	1.04, 4.14, 7.4	304	0.59, 1.37, 1.7	18.649		0.71	[26]
	1.17, 7.4	342.6	0.31, 1.2				[26]
	1.39, 5.19, 20.6	307.8	0.69, 1.49, 2.3		20		[35]
	0.93	296.07	0.65	21-21.5	20.9		[84]
	1	297	0.70	21	21		[34]
	1.01, 4.86	313	0.55, 1.5				[32]
SrY	1.1, 4.86, 53.2	298	0.6, 1.66, 4.2				[36]
Zn-dabco	6.25, 50, 100	303	3.75, 8.44, 8.8				[8]
ZSM-22		309			27.2		[25]
ZSM-5		297.15			21.0		[25]

Among the Zeolitic adsorbents *viz.* X, Y, A, ZSM, silicalite etc. we could easily see a similar trend with less variation in the amount adsorbed at the same experimental conditions. As a matter of fact if we summarize our findings for pressures ranging from 1-5 bar and temperatures ranging from 298-305 K, we have found that for 5A zeolite the amount adsorbed varied between 0.77~1.8 mmol g^{-1}, whereas for Y-type zeolite *viz.* the corresponding figures are 0.65~1.8 (BaY), 0.57~1.95 (CaY), 0.4~1.69 (MgY), 0.31~1.59 (NaY), 0.6~1.66 mmol g^{-1}(SrY) respectively. The available data at 1 bar pressure for NaX (0.6 mmol g^{-1}), Na-ZSM-5 (0.7 mmol g^{-1}), Na-ETS-4 (0.54 mmol g^{-1}), silicalite (0.59 mmol g^{-1}) lie very close to their counterparts as well.

For carbonaceous adsorbents *viz.* activated carbon (AC), the adsorbed capacity for CH_4 lies close to zeolites. From the available data at 3 bar pressure and 298 K, the adsorbed capacity is *ca.* 2.4 mmol g^{-1}(AC, BPL); *ca.* 1.75 mmol g^{-1} (AC, Centaur); *ca.* 1.7 (AC, Norit R1).

Coming to new generation of adsorbents *viz.* metal organic frameworks the corresponding loading values are a few notches higher. For example, Cu-BTC at 298 K and pressure up to 5 bar reported to adsorb *ca.* 5 mmol g^{-1}. The values are more or less similar for Cr based (MIL series) and Zn based (IRMOFs) as well.

From the preceding discussion it is amply clear that CH_4 adsorption is largely dictated by the surface area possessed by various adsorbents and not by the polarity of the adsorbent surfaces. Methane being a non-polar molecule with zero dipole moment, the logic sounds stronger. This is probably the reason why even though there is a wide variation in the surface characteristics of individual zeolites (A, X, Y, ZSM-5, silicalite) and between zeolite and activated carbon, but since their surface area lies closer to 300 to 800 m^2 g^{-1}, they have similar affinities and hence the adsorption capacity.

Contrary to zeolites and activated carbons, MOFs are reported to have larger void spaces or specific surface areas, to the tune of 1500 to 3500 m^2 g^{-1}. Thus, the higher capacity in the gas uptake could be largely attributed to that only.

5.2 Isotherm Model Fits

Langmuir isotherm model is used to fit the experimental data. The experimental data are shown the appendix II. Two characteristically different adsorbents were picked for our present study, microporous Cu-BTC (or, HKUST-1) and mesoporous Cr-BDC (or, MIL-101). The modelling results and model fits are given in the respective figures and tables.

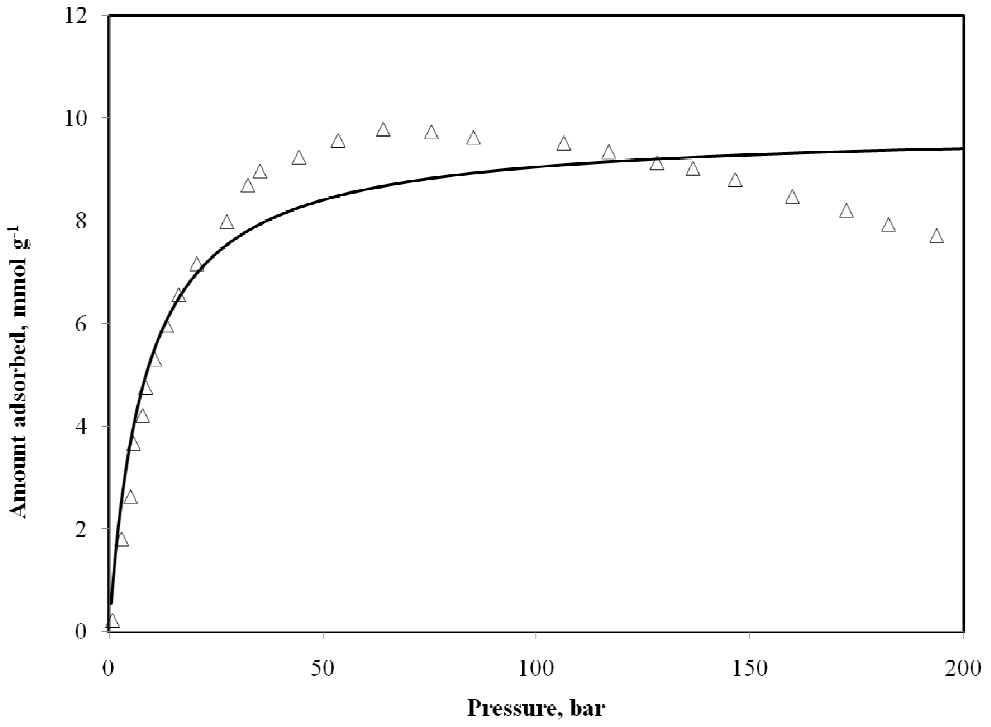

Figure 5.1: Adsorption isotherm of CH_4 on Cu-BTC. Open symbols: Experimental data points [41]. Solid line: Langmuir model.

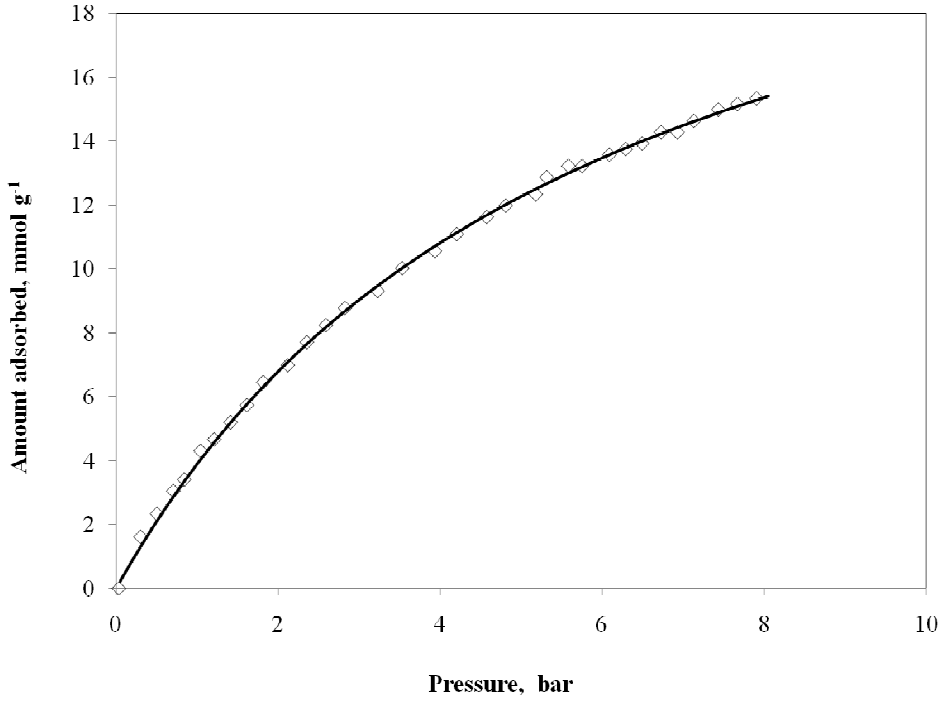

Figure 5.2: Adsorption isotherm of CH_4 on Cr-BDC. Open symbols: Experimental data points [9]. Solid line: Langmuir model.

Table 5.2: Langmuir model parameters

Adsorbents	Langmuir Model Parameters		R-square
	N^{max} (mmol g^{-1})	H (mmol g^{-1} bar^{-1})	
Cu-BTC	9.795	1.182	0.9129
Cr-BDC	26.51	4.565	0.9989

Figure 5.1 illustrates the modelling of CH_4 adsorption on Cu-BTC. Since the experimental data for this particular case was available to a very high pressure, the Langmuir model could only best-fit the low pressure regime and is evident from R-square value. The saturation loading for this particular case is approximately 9.795 mmol g^{-1}, and Henry constant is 1.182 mmol g^{-1} bar^{-1}. Similarly for Cr-BDC, the values are 26.51 mmol g^{-1} and 4.565 mmol g^{-1} bar^{-1} respectively. A very high saturation loading for Cr-BDC can be attributed to its very high surface area as compared to Cu-BTC. For example, Cr-BDC for this particular case is reported to have ca. 3200 m^2 g^{-1} specific surface area which is way above 1500 m^2 g^{-1} for Cu-BTC. As a matter of fact, it does appear that a convenient 'scaling factor' can be used to compare between the respective adsorption capacities (which are the ratio of surface area).

Additionally, if we shift our attention to the low pressure regime i.e. between 0 and 1 bar pressure, we observe contrasting scenarios. In case of Cu-BTC, the slope of the curve in the low pressure region is very sharp as compared to Cr-BDC. This anomaly can be attributed to the presence of multiple adsorption sites. A thorough fact finding literature survey indicates that in case of Cr-BDC, two different preferential adsorption sites are available. The first being the Cr^{+3} metal sites and the second, being the super-tetrahedra site. During synthesis of Cr-BDC, benzene dicarboxylic acid forms as a by-product. It is a known fact that they tend to poison the metal sites and hence a through post-synthesis treatment becomes very crucial to get rid of all the solvated impurities. In most gas-solid interactions, preferential adsorption takes place at around any metal centres or sites. In case of Cr-BDC, due to poisoning or blocking metal sites by BDC molecule leads to the availability of lesser number of metal sites. And hence, metal sites become fast saturate and most of the adsorption does take place at the super-tetrahedra site and that is reflected in the isotherm. Conversely, Cu-BTC is known for their clean metal sites, devoid of any such poisoning/blocking and that leads to a greater interaction in the low-pressure zone.

CHAPTER 6

Conclusions and Future Scope

In our present research we have successfully carried out CH_4 adsorption study on various industrially important adsorbents with special emphasis on MOFs. Langmuir isotherm model was used to fit the experimental data. A comprehensive table was made after reviewing various research articles on CH_4 adsorption. We think such a study is crucial in creating a database for any future reference. Being a non-polar molecule, we found that it is the surface area which plays a pivotal role in adsorption of methane. Cr-BDC metal organic framework is found to be the most suitable adsorbent.

There requires a lot to be done as an extension of this work. More sophisticated isotherm models should be used to explore and explain the gas-solid interaction at the molecular level. Since there remain an ambiguity on published data on gas adsorption on MOFs, it is always practical to synthesize and carry out high pressure gas adsorption measurements in the same laboratory using any suitable gravimetry and volumetry techniques.

APPENDIX I

Derivation of Langmuir Model

Equation relating amount of gas adsorbed and pressure is given by

$$N = \frac{N^{max} HP}{N^{max} + HP} \quad \text{(E.q 1)}$$

Where,

H-Henry's Constant, which is temperature dependent

$H=H_0e^{-H_1/T}$ (E.q 2)

H_0 is an Enthalpy dependent term

(E.q 1) is rewritten as

$N*N^{max}+N*H*P=N^{max}*H*P$ (E.q 3)

$P = (N*N^{max})/H *(N^{max}-N)$(E.q 4)

Applying ln to the (E.q 4)

$\ln P =\ln(N*N_{max})-\ln\{H*(N_{max}-N)\}$

$=\ln N+\ln N_{max}-\ln H-\ln(N_{max}-N)$ (E.q 5)

Applying H from (E.q 2) in (E.q 5) and differentiating w.r.t 1/T, we get

$\partial(\ln P)/\partial(1/T) =H_1$ (E.q 6)

Multiplying by -R on both sides of (E.q 6)

$-R\partial(\ln P)/\partial(1/T) =-RH_1$

But

$-\Delta h_{ads} =R\partial(\ln P)/\partial(1/T)$

So $-\Delta h_{ads}= -RH_1$

$-\Delta h_{ads}/R = H_1$

Isosteric Heat = RH_1 which is profoundly knows as Vant Hoff equation

APPENDIX II

(A) Adsorption data on CH_4 adsorption on Cu-BTC [41]

T	P	N	N
	(bar)	(g g^{-1})	(mmol g^{-1})
303 K	0.70	0.003	0.219
	2.82	0.029	1.803
	4.93	0.042	2.623
	5.63	0.059	3.661
	7.75	0.067	4.208
	8.45	0.076	4.754
	10.56	0.085	5.301
	13.38	0.095	5.956
	16.20	0.105	6.558
	20.42	0.115	7.159
	27.47	0.128	7.978
	32.39	0.139	8.689
	35.21	0.143	8.962
	44.37	0.148	9.235
	53.52	0.153	9.563
	64.09	0.157	9.781
	75.35	0.156	9.727
	85.21	0.154	9.618
	106.34	0.152	9.508
	116.90	0.150	9.344
	128.17	0.146	9.126
	136.62	0.144	9.016
	146.48	0.141	8.798
	159.86	0.136	8.470
	172.54	0.131	8.197
	182.39	0.127	7.924
	193.66	0.123	7.705

(B) Adsorption data on CH_4 adsorption on Cr-BDC [9]

T	P	N	N
	(bar)	(cm^3g^{-1})	(mmol g^{-1})
	6.92	85.816	3.8286785
	13.282	136.54	6.0917284
	17.147	148.4	6.620862
	22.944	166.72	7.4382083
	27.457	179.12	7.9914339
	31.321	191.52	8.5446596
	35.838	202.29	9.0251628
	44.911	209.26	9.3361292
	53.984	216.23	9.6470956
303 K	65.016	218.87	9.7648791
	76.058	217.73	9.714018
	87.751	216.05	9.6390649
	105.94	212.17	9.4659588
	116.99	207.79	9.2705452
	128.04	202.87	9.0510395
	135.2	199.05	8.8806103
	146.9	193.59	8.6370126
	171.61	180.5	8.0530026
	196.31	169.03	7.5412688

REFERENCES

[1] Yang, R. T., *Gas Separation by Adsorption Processes*, Imperial College Press, London (1997), Chapter-1.

[2] Ruthven, D. M. and Sun, M. S., *Principle of Adsorption and Adsorption Processes*, Wiley-Interscience, New York, (1984), Chapter-1.

[3] Barton, T. J., Bull, L. M., Klemperer, W. G., Loy, D. A., McEnaney, B., Misono, M., Monson, P. A., Pez, G., Scherer, G. W., Vartuli, J. C., and Yaghi, O. M., "Tailored Porous Materials," *Chem. Mater.*, 11, 2633-2656 (1999).

[4] Vishnyakov, A., Ravikovitch, P. I., Neimark, A. V., Bülow,M., Wang, Q. M.,"Nanopore structure and sorption properties of Cu-BTC metal-organic framework," *Nano Lett.*, 3, 713-718 (2003).

[5] Yang, Q., Xue, C., Zhong, C., and Chen, J. –F.,"Molecular Simulation of Separation of CO_2 from Flue Gases in Cu-BTC Metal-Organic Framework," *AIChE J.*, 53, 2832-2840 (2007).

[6] Eddaoudi, M., Kim, J., Rosi, N., Vodak, D., Wachter, J., O'Keeffe, M., Yaghi, O. M.," Systematic Design of Pore Size and Functionality in Isoreticular MOFs and Their Application in Methane Storage," *Science*, 295, 469-472 (2002).

[7] Bourrelly, S., Llewellyn, P. L., Serre, C., Millange, F., Loiseau, T., and Férey, G., "Different Adsorption Behaviors of Methane and Carbon Dioxide in the Isotypic Nanoporous Metal Terephthalates MIL-53 and MIL-47," *J. Am. Chem. Soc.*, 127, 13519-13521 (2005).

[8] Millward, A. R., and Yaghi, O. M.," Metal-Organic Frameworks with Exceptionally High Capacity for Storage of Carbon Dioxide at Room Temperature," *J. Am. Chem. Soc.*, 127, 17998-17999 (2005).

[9] Senkovska, I. and Kaskel, S.," High pressure methane adsorption in the metal-organic frameworks $Cu_3(btc)_2$, $Zn_2(bdc)_2dabco$, and $Cr_3F(H_2O)_2O(bdc)_3$," *Micropor. Mesopor. Mater.*, 112, 108-115 (2008).

[10] Rosi, N. L., Eckert, J., Eddaoudi, M., Vodak, D. T., Kim, J., O'Keeffe, M., and Yaghi, O. M.," Hydrogen Storage in Microporous Metal-Organic Frameworks," *Science*, 300, 1127-1129 (2003).

[11] Rowsell, J. L. C., Millward, A. R., Park, K. S., and Yaghi, O. M.," Hydrogen Sorption in Functionalized Metal-Organic Frameworks," *J. Am. Chem. Soc.*, 126, 5666-5667 (2004).

[12] Wong-Foy, A. G., Matzger, A. J., and Yaghi, O. M., "Exceptional H_2 Saturation Uptake in Microporous Metal-Organic Frameworks," *J. Am. Chem. Soc.*, 128, 3494-3495 (2006).

[13] Pan, L., Sander, M. B., Huang, X., Li, J., Smith, M., Bittner, E., Bockrath, B., and Karl Johnson, J.," Microporous Metal Organic Materials: Promising Candidates as Sorbents for Hydrogen Storage," *J. Am. Chem. Soc.*, 126, 1308-1309 (2004).

[14] Férey, G., Latroche, M., Serre, C., Millange, F., Loiseau, T., and Percheron-Guégan, A., "Hydrogen adsorption in the nanoporous metal-benzenedicarboxylate $M(OH)(O_2C–C_6H_4–CO_2)$ ($M = Al^{3+}$, Cr^{3+}), MIL-53," *Chem. Commun.*, 2976-2977 (2003).

[15] Latroche, M., Surblé S., Serre, C., Mellot-Draznieks, C., Llewellyn, P. L., Lee, J. H, Chang, J. S., Jhung, S. H., and Férey, G., "Hydrogen Storage in the Giant-Pore Metal-Organic Frameworks MIL-100 and MIL-101," *Angew. Chem. Int. Ed.*, 45, 8227-8231 (2006).

[16] Li, Y., and Yang, R. T.," Significantly Enhanced Hydrogen Storage in Metal-Organic Frameworks via Spillover," *J. Am. Chem. Soc.*, 128, 726-727 (2006).

[17] Li, Y., and Yang, R. T., "Hydrogen Storage in Metal-Organic Frameworks by Bridged Hydrogen Spillover," *J. Am. Chem. Soc.*, 128, 8136-8137 (2006).

[18] Li, Y., and Yang, R.T., "Hydrogen Storage in Metal-Organic and Covalent-Organic Frameworks by Spillover," *AIChE J.*, 54, 269-279 (2008).

[19] Panella, B., Hirscher, M., Putter, H., and Muller, U.," Hydrogen Adsorption in Metal–Organic Frameworks: Cu-MOFs and Zn-MOFs Compared," *Adv. Funct. Mater.*, 16, 520-524 (2006).

[20] Lebedev, O. I., Millange, F., Serre, C., Van Tendeloo, G., and Férey, G.," First Direct Imaging of Giant Pores of the Metal-Organic Framework MIL-101," *Chem. Mater.*, 17, 6525-6527 (2005).

[21] Vermesse, J., Vidal, D., and Malbrunot, P., "Gas Adsorption on Zeolites at High Pressure," *Langmuir*, 12, 4190-4196 (1996).

[22] Salem, M.M.K., Braeuer, P., Szombathely, M.V., Heuchel, M., Harting, P., Quitzsch, K., and Jaroniec, M., "Thermodynamics of High-Pressure Adsorption of Argon, Nitrogen, and Methane on Microporous adsorbents," *Langmuir*, 14, 3376-3389 (1998).

[23] Liu, J., Culp, J.T., Natesakhawat, S., Bockrath, B.C., Zande, B., Sankar, S.G., Garberoglio, G., and Karl Johnson, J., "Experimental and Theoretical Studies of Gas Adsorption in $Cu_3(BTC)_2$: An Effective Activation Procedure," *J. Phys. Chem. C.*, 111, 9305-9313 (2007).

[24] Pillai, R.S., Peter, S.A., and Jasra, R.V., "Adsorption of carbon dioxide, methane, nitrogen, oxygen and argon in NaETS-4," *Micropor. Mesopor.Mater.*, 113, 268-276 (2008).

[25] Dunne, J.A., Rao, M., Sircar, S., Gorte, R.J., and Myers, A.L.," Calorimetric Heats of Adsorption and Adsorption Isotherms. 2. O_2, N_2, Ar, CO_2, CH_4, C_2H_6, and SF_6 on NaX, H-ZSM-5, and Na-ZSM-5 Zeolites," *Langmuir*, 12,5896-5904 (1996).

[26] Myers, A.L., "Characterization of nanopores by standard enthalpy and entropy of adsorption of probe molecules," Colloids and Surfaces A, 241, 9-14 (2004).

[27] Dunne, J.A., Mariwala, R., Rao, M., Sircar, S., Gorte, R.J., and Myers A.L., "Calorimetric Heats of Adsorption and adsorption Isotherms.1. O_2, N_2, Ar, CO_2, CH_4, C_2H_6, and SF_6 on Silicalite," *Langmuir*, 12, 5888-5895 (1996).

[28] Talu, O., Li, J., Kumar, R., Mathias, P.M., Moyer, J.D., Jr, and Schork, J.M., "Measurement and analysis of oxygen/nitrogen/5A-zeolite adsorption equilibria for air separation," *Gas. Sep. Purif.*, 10, 149-159 (1996).

[29] Frère, M.G., and De Weireld, G.F., "High-Pressure and High-Temperature Excess Adsorption Isotherms of N_2, CH_4, and C_3H_8 on Activated Carbon," *J. Chem. Engg. Data,* 47, 823-829 (2002).

[30] Shen, D., and Bülow, M., "Comparison of Experimental Techniques for Measuring Isosteric Heat of Adsorption," *Adsorption*, 6, 275-286 (2000).

[31] García-Pérez, E., Gascón, J., Morales-Flórez, V., Castillo, J.M., Kapteijn, F., and Calero, S., "Identification of Adsorption sites in Cu-BTC by Experimentation and Molecular Simulation," *Langmuir*, 25, 1725-1731 (2009).

[32] Li, P., and Tezel, F.H.,"Pure and Binary Adsorption Equilibria of Carbon Dioxide and Nitrogen on Silicalite, " *J. Chem. Engg. Data,* 53, 2479-2487 (2008).

[33] Li, P., and Tezel, F.H., "Pure and Binary Adsorption of Methane and Nitrogen by Silicalite," *J. Chem. Engg. Data,* 54, 8-15 (2009).

[34] Zhao, Z., Li, Z., and Lin, Y.S., "Adsorption and Diffusion of Carbon Dioxide on Metal-Organic Framework (MOF-5)," *Ind. Eng. Chem. Res.*, 48, 10015-10020 (2009).

[35] Siperstein, F.R., and Myers, A.L., "Mixed-Gas Adsorption," *AIChE J.*, 47, 1141-1159 (2001).

[36] Sun, M.S., Shah, D. B., Xu, H. H., and Talu, O., "Adsorption Equilibria of C_1 to C_4 Alkanes, CO_2, and SF_6 on Silicalite," *J. Phys. Chem. B*, 102, 1466-1473(1998).

[37] Talu, O., Zhang, S.-Y., and Hayhurst, D.T., "Effect of Cations on Methane Adsorption by NaY, MgY, CaY, SrY, and BaY Zeolites," *J. Phys. Chem.*, 97, 12894-12898 (1993).

[38] Garberoglio, G., Skoulidas, A.I., and Karl Johnson, J., "Adsorption of Gases in Metal Organic Materials: Comparison of Simulations and Experiments," *J. Phys. Chem. B*, 109, 13094-13103 (2005).

[39] Wang, S., "Comparative Molecular Simulation Study of Methane adsorption in Metal-Organic frameworks," *Energy & Fuels*, 21, 953-956 (2007).

[40] Do, D. D., *Adsorption Analysis: Equilibria and Kinetics*, Imperial College Press, London, 1998.

[41] Schlichte, K., Kratzke, T., and Kaskel, S.,"Improved synthesis, thermal stability and catalytic properties of the metal-organic framework compound $Cu_3(BTC)_2$," *Micropor. Mesopor. Mater.*, **73**, 81-88 (2004).